COMPUTER-AIDED DESIGN & APPLICATIONS, 2018
VOL. 15, NO. 3, 353–366
https://doi.org/10.1080/16864360.2017.1397886

Model-based next-best-view planning of terrestrial laser scanner for HVAC facility renovation

Eisuke Wakisaka [a], Satoshi Kanai [b] and Hiroaki Date [b]

[a]Shinryo Corporation, Japan; [b]Hokkaido University, Japan

ABSTRACT

Recently, terrestrial laser scanners (TLSs) have been introduced to efficient as-built three-dimensional (3D) modeling in the heating, ventilating, and air-conditioning (HVAC) industry. When scanning the highly tangled installation of piping objects in HVAC systems using TLS, it is difficult to manually decide feasible scanner placement to scan the necessary regions of objects for construction with high accuracy and high point density and without any occlusion. Therefore, in this paper, we propose a model-based next-best-view planning method for TLS. The method uses a coarse 3D model generated by structure-from-motion (SfM), and it finds the near-optimum scanner placement that maximizes scan coverage while satisfying the constraints on the factors influencing scan quality such as beam incident angle, scan range, and scan overlap. The constraints are imposed based on user-specified scanning priority levels. Scanner placement is determined based on voxel-based space occupancy classification. The superiority of scanner placement by using the proposed method is verified through a comparative evaluation of the modeling accuracy with scanner placement by an experienced operator.

KEYWORDS

next-best-view planning; laser scanning; structure-from-motion

1. Introduction

Recently, building facility renovations have been increasing in the heating, ventilating, and air-conditioning (HVAC) industry. Therefore, efficient and accurate construction planning is needed in the planning phase of such projects. In HVAC facility renovation works, given that some parts of old facilities such as heating machines and connecting pipes are removed and replaced with new parts, it is necessary to identify the exact locations of the existing old facilities on-site and design new facilities that can be retrofitted perfectly. To this end, we need on-site laser scanning and as-built modeling based on laser-scanned points data. The reconstruction of as-built three-dimensional (3D) models of HVAC facilities by laser scanning using a terrestrial laser scanner (TLS) has shortened survey periods and facilitated in-depth construction planning. To this end, automatic recognition and as-built modeling of air-conditioning ducts and piping objects from laser-scanned point clouds have been studied [1], [15].

Usually, equipment, ducts, and piping objects of HVAC facilities are installed in a very tiny space in a highly tangled manner. Therefore, it is difficult even for experienced operators to find a feasible scanner placement that fulfills the quality requirements of measurement accuracy, scan point density, and scan coverage.

The accuracy of laser-scanned points depends primarily on the incident angle of the laser beam on the object surfaces and on the scan range of the scanner [19]. For registration, there must be a certain amount of overlap among the scanned points. Therefore, to find feasible scanner placement, the upper and the lower bounds of the beam incident angle, scan range, and scan overlap should be considered as constraints on factors influencing quality.

The degree of scan quality required differs considerably by region, object, or type of construction work. Accordingly, the constraints on the factors influencing quality differ. For example, flanges and valves connecting equipment and pipes must be scanned with very precise positional information, while the regions around the equipment do not necessarily need to be scanned with high accuracy. Therefore, feasible scanner placement should also consider the complex constraints on the factors influencing quality, which vary from object to object. Moreover, in determining the optimum scanner placement, the amount of space occluded from the scanners should be minimized. In other words, the scan coverage should be maximized.

CONTACT Eisuke Wakisaka wakisaka.ei@shinryo.com; Satoshi Kanai kanai@ssi.ist.hokudai.ac.jp; Hiroaki Date hdate@ssi.ist.hokudai.ac.jp

Currently, scanner placement is completely determined by experienced operators. However, there is no guarantee that the placement determined by the operators fulfills the required constraints on the factors influencing quality nor is the scan coverage maximized. Therefore, a computer-aided approach is needed to find the optimal sequence of TLS setup positions, that is, the optimum scanner placement that completely satisfies the required scan quality and maximizes the scan coverage simultaneously.

The problem of finding the optimal sensor placement is called next-best-view (NBV), and many solutions to this problem have been proposed. These solutions are classified into two types: model-based methods that use an initial model of the objects to be scanned and non-model-based methods that use no prior knowledge about the objects [17]. Several non-model-based NBV planning methods for TLSs have already been proposed [13], [21]. However, these studies do not deal with the constraints on the factors influencing scan quality such as incident angle, scan range, and scan overlap because they employ non-model-based methods for planning. By contrast, several model-based NBV planning methods for TLSs using a two-dimensional (2D) drawing of a building as *a priori* knowledge have been proposed [2], [4], [6], [20]. However, these as-built drawings may not be consistent with the current state of the object to be scanned. Moreover, the planning in these studies was 2D, which does not allow for estimation of scanner placement from the viewpoint of minimizing 3D occlusions in HVAC facilities.

To solve the issues, in this paper, we propose a new model-based NBV planning method for a TLS by using a coarse 3D model constructed from structure-from-motion (SfM) as *a priori* knowledge. The method finds a near-optimum scanner placement that maximizes scan coverage while satisfying the constraints on the factors influencing scan quality such as beam incident angle, scan range, and scan overlap. The constraints are user-specified scanning priority level. Scanner placement is determined using voxel-based space occupancy classification and ray casting. The superiority of scanner placement using the proposed method is verified through a comparative evaluation of the modeling accuracy of scanner placement by an experienced operator.

2. Related work and contributions

2.1. Related work

Scan quality, such as point density and measurement accuracy, is the most important requirement in laser scanning projects for as-built 3D modeling. The quality of point clouds in laser scanning is influenced greatly by instrument calibration, atmospheric conditions, object properties, and scanning geometry [19]. Among them, scanning geometry refers to geometric factors that influence scan quality, and they mainly include beam incident angle, scan range, and point density at each scan point, which is determined relatively by the orientation of the scanned surface and the scanner position. The influence of these factors on measurement accuracy has been investigated experimentally by using various TLSs [5], [14]. In these studies, it has been shown that increasing the incident angle and scan range lowers the measurement accuracy.

Many NBV methods have been proposed in robotics [4], reverse engineering [16], [17], plant engineering [13], and architecture and building construction [2], [6], [20], [21]. For comprehensive reviews of NBV solutions, see Scott *et al.* [17] and Wujanz *et al.* [22]. Among them, in non-model-based NBV methods [16], [17] for reverse engineering, the objects to be scanned have relatively simple geometries, such as cups and sculptures, and they are placed in an uncluttered space. The object size is smaller than the scan range of the sensor, and the sensor is located outside and close to the objects. By contrast, in laser scanning projects of HVAC facilities, the space to be scanned is highly tangled and cluttered, and it is generally much wider than the space that can be captured in one scan. The laser scanner is usually located inside the space to be scanned. Therefore, these conventional NBV methods are unsuitable for estimating optimal scanner placement in laser scanning projects of HVAC facilities.

The scenarios of other non-model-based NBV methods [8], [13], [21] for plant piping objects or large-scale outdoor settings by using a TLS are similar to that of the 3D scanning of HVAC facilities. However, despite the fact that optimal scanner setup positions can be determined sequentially by using these NBV methods, the constraints on the factors influencing scan quality such as incident angle, scan range, and scan overlap are ignored because these NBV methods are non-model-based, object surfaces to be scanned in unmeasured regions are basically unknown, and the factors influencing quality cannot be estimated.

Model-based NBV methods for scanning large-scale indoor or outdoor scenes by using 2D drawings as *a priori* knowledge have been proposed [2], [4], [6], [20]. Most such methods facilitate optimal scanner placement by considering the factors influencing scan quality. However, the objects to be scanned consist of relatively simple-shaped buildings. If these methods are applied to the laser scanning of HVAC facilities, full scan coverage cannot be necessarily guaranteed because such facilities are characterized by highly tangled 3D installations and 3D

occlusions among objects, which cannot be estimated correctly from the viewpoint of scanner placement by using only 2D drawings. Kitada *et al.* [12] recently proposed an NBV solution for scanning large-scale outdoor buildings by using a coarse 3D model constructed using SfM. Although their method satisfies the point cloud density constraint, it ignores the factors influencing scan quality.

2.2. Our contributions

Different from the previous studies, the contributions of our proposed NBV method are as follows:

- We propose a novel model-based NBV algorithm specialized for HVAC renovations that can automatically determine near-optimum scanner placement. This maximizes scan coverage while completely satisfying the constraints on the factors influencing scan quality such as beam incident angle, scan range, and scan overlap.
- A novel SfM technique is introduced to estimate the approximated object model, which is then used to correctly examine the visibility of the object from a scanner position based on spatial occupancy.
- We verify how the proposed constraints on incident angle, scan range, and scan overlap ratio affect the final scanner placement according to the scanning priority level.
- We evaluate the difference in scan quality between scanner placement obtained using the proposed NBV method and that determined by an experienced operator.
- We experimentally evaluate how the optimal scanner placement obtained using the proposed NBV method effectively increases the accuracy of as-built 3D modeling.

3. Model-based NBV planning algorithm for TLS

3.1. Overview of the proposed method

The proposed NBV method consists of the following six steps, as shown Fig. 1:

- A coarse 3D model (SfM model) of the space to be scanned is constructed using SfM software from multiple photos taken during a preliminary survey (A1).
- The space covered by the SfM model is decomposed into a set of voxels, and the spatial occupancy of each voxel is classified by ray casting at the camera positions already estimated using SfM software (A2).
- A scanning priority level that differs across regions in the SfM model depending on the construction type is assigned manually to the voxels interactively (A3).
- Practical scanner setup position candidates are estimated based on the spatial occupancy of the voxels (A4).
- Scan target voxels are identified based on each camera position (A5).
- A near-optimal sequence of scanner setup positions is extracted from the position candidates to maximize the scan coverage while satisfying the constraints on factors influencing scan quality, such as incident angle, scan range, and scan overlap, by using the greedy method (A6).

The details of the method are described in the following sections.

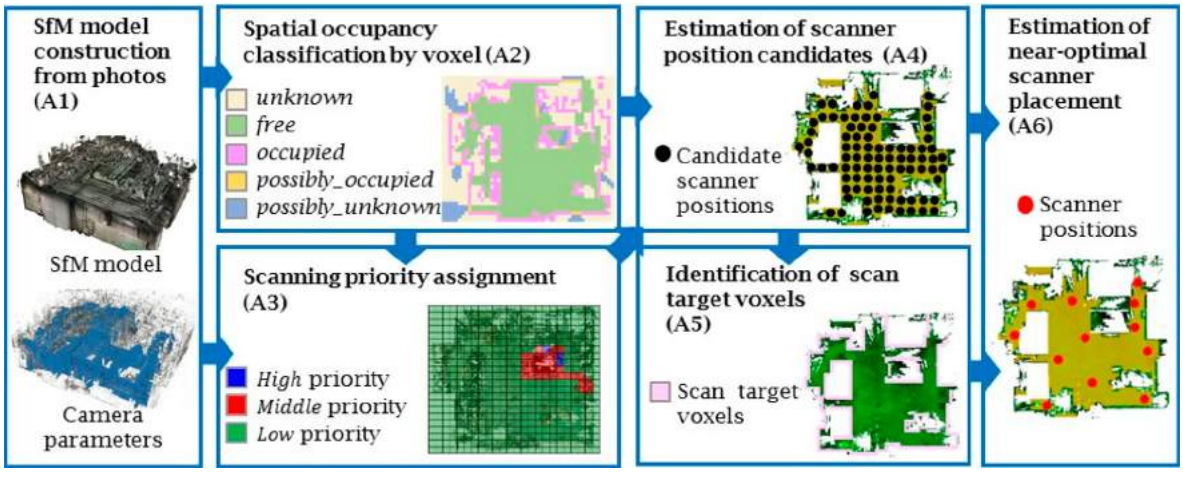

Figure 1. Overview of proposed method.

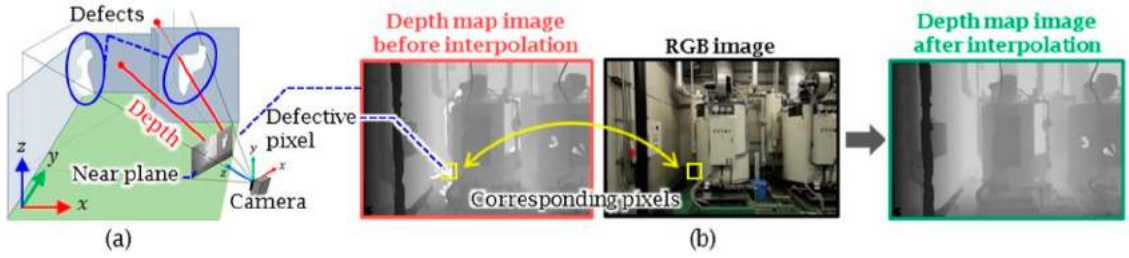

Figure 2. Generation of depth map and interpolation of depths of defective pixels.

3.2. SfM model construction from photos (A1)

To obtain *a priori* knowledge of the space to be scanned, an SfM model is generated from multiple photos by using commercial SfM software [7]. SfM is a 3D modeling method that simultaneously constructs a textured 3D model from a large collection of photos and estimates the camera positions and orientations (extrinsic parameters) corresponding to each photo. These extrinsic parameters are used in steps A2 and A5. However, when applying SfM to indoor HVAC facilities, the SfM model tends to be incomplete and includes a few defects such as holes owing to the lack of feature points in the photos. Because false classifications occur when spatial occupancy is classified using this model with defects and a poor scanner position might be obtained, we have rectified these defects in our algorithm, as described in A2.

3.3. Spatial occupancy classification by voxel (A2)

When planning the optimal scanner placement, the free or occupied status of the space to be scanned must be determined. Hence, as shown in Fig. 2, the space enclosing the SfM model is decomposed into a set of voxels with the spatial resolution l_v, and a spatial occupancy attribute is classified and assigned to each voxel by ray casting.

In this classification, first, to rectify the defects in the SfM model, as shown in Fig. 2(a), a depth map image with depth equaling the distance from the near plane to the SfM model surface is generated at a camera position. The depth value of a defective pixel tends to be extremely higher than that of a normal pixel.

Next, as shown in Fig. 2(b), depth values of defective pixels in the depth map image are interpolated using the depth values of the neighboring pixels based on color similarity among RGB image pixels. We adopted the depth map-restoring approach proposed by Bapat *et al.* [3]. Then, as shown in Fig. 3(a), the space enclosing the SfM model is decomposed into a set of voxels with the spatial resolution l_v. The interpolated depth in the depth map image at each camera position is back-projected to a particular voxel in this voxel space. Then, the view frustum is generated according to the extrinsic parameters of the camera, and the outmost voxel centroid P_{end} contained in the view frustum is extracted.

Finally, ray casting, as shown in Fig. 3(b), is performed between the projection centers of the camera P_{cam} and every outmost voxel centroid P_{end}. The ray connecting P_{cam} and P_{end} is defined as r, and the spatial occupancy of a voxel V_r penetrated by r is checked sequentially in order from P_{cam} to P_{end}. Thereafter, a spatial occupancy attribute $a(v) \in \{free, occupied, unknown, possibly\_occupied, possibly\_unknown\}$ is assigned to voxel v.

As shown in Fig. 3(c), $a(v) = free$ indicates that a ray from the camera has already passed through voxel v and that v contains no object. Furthermore, $a(v) = occupied$ indicates that v contains a surface of the SfM model. $a(v) = unknown$ indicates that a ray from the camera

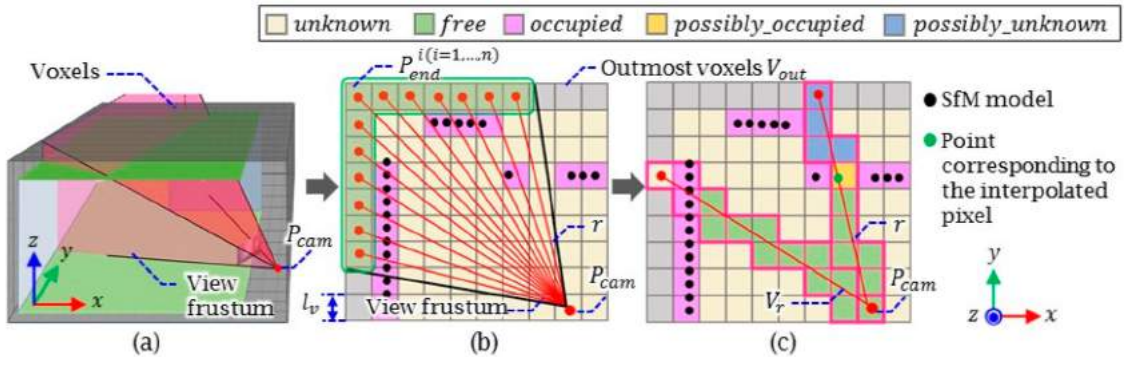

Figure 3. Spatial occupancy classification.

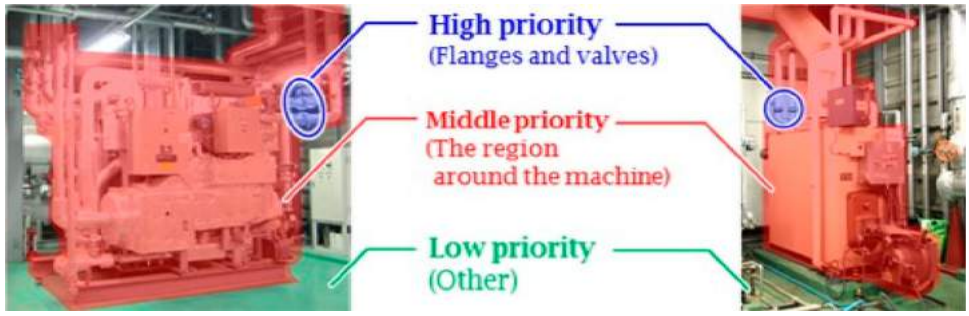

Figure 4. Scanning priority levels.

has not yet passed through v because it is blocked by an *occupied* voxel. Moreover, $a(v) = possibly\_occupied$ means that v contains a point corresponding to the interpolated depth of a defective pixel and we cannot uniquely determine the occupancy attribute of v as either *occupied* or *free*. Similarly, $a(v) = possibly\_unknown$ means that we cannot uniquely determine the occupancy attribute of the voxel as either *unknown* or *free* because v is placed behind the other *possibly_occupied* voxel on the front, and the occupancy attribute of v may change depending on whether the voxel in front is *occupied* or *free*.

Initially, $a(v) = unknown$ is assigned to all voxels. By executing the above-mentioned processing at every camera position, the spatial occupancy of the entire voxel space is classified and assigned.

3.4. Scanning priority assignment (A3)

In facility construction, the required scan quality differs by region depending on the construction type. Therefore, in our method, we introduce scan priority level to specify the degree of scan quality, and this scan priority level can be used to control the bounds of constraints on the factors influencing quality.

For example, as shown in Fig. 4, in the case of a laser scan for updating equipment, the flanges and valves connecting the equipment and the pipes should be assigned *high* priority because their scanned points must have precise positional information and a high degree of scan quality. In contrast, the regions around the equipment should be assigned *middle* priority because interference between the new pipes and the equipment must only be inspected with a modest degree of scan quality. The remaining regions are assigned *low* priority, and they need not be measured.

In priority assignment, first, the SfM model is manually segmented into several regions by using point-cloud-processing software [10]. Then, one of the scanning priority levels, $b(v) \in \{high, middle, low\}$, is assigned interactively to each occupied voxel v_{occ} included in each segmented region.

3.5. Estimation of scanner position candidates (A4)

After the scanning priority level is assigned, a set of candidates for the next scanner setup positions is extracted from the voxel space in which a scanner can be placed practically. We assume that the candidates for scanner positions meet the condition that a TLS body can be placed stably on a ground surface without interfering with piping objects.

For finding the candidates, first, the average normal of the faces on the SfM model in a voxel $\boldsymbol{n}_s$ is estimated. Next, a voxel whose normal vector points vertically upwards $\boldsymbol{n}_z$ is extracted as the *floor* voxel from the *occupied* voxels ($a(v) = occupied$). Subsequently, the connected *floor* voxels are clustered using Euclidean clustering.

To find the candidate scanner positions, as shown in Fig. 5, the shape of the laser scanner body, including the tripod, is approximated as an enclosed cylinder C_{scan} with the scanner base radius r_{scan}. Then, only the subset of the *floor* voxels on which the scanner can be placed is extracted according to the following two conditions. The first is that the area of the connected *floor* voxels must be sufficiently large to place the scanner. According to this condition, the voxels contacting the bottom of C_{scan} are *occupied* ($a(v) = occupied$) or *possibly_occupied* ($a(v) = possibly\_occupied$). The second is that C_{scan} should not include any *occupied* voxel within it to avoid collisions between the scanner body and other objects. Then, a *free* voxel located on the axis of C_{scan} with a height equaling the scanner origin height h_{scan} is selected as a candidate scanner position voxel v_c. By collecting all v_c at every C_{scan} in the voxel space, a set of scanner position candidate voxels V_c is finally determined.

3.6. Identification of scan target voxels (A5)

Next, the *occupied* voxels that are invisible from any camera position are excluded, and the voxels that are assigned *high* or *middle* priority and are visible from a camera position are identified as the scan target voxels.

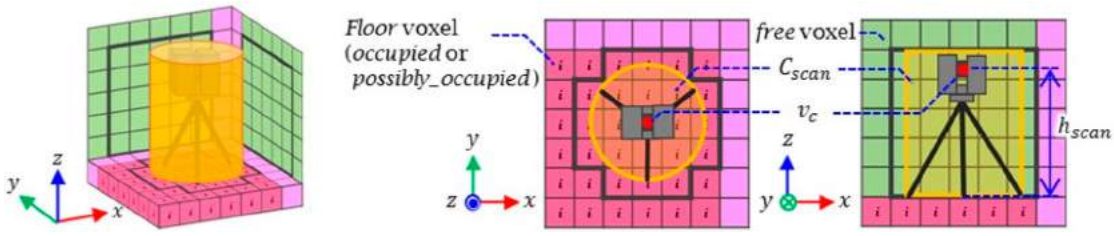

Figure 5. Candidate scanner positions.

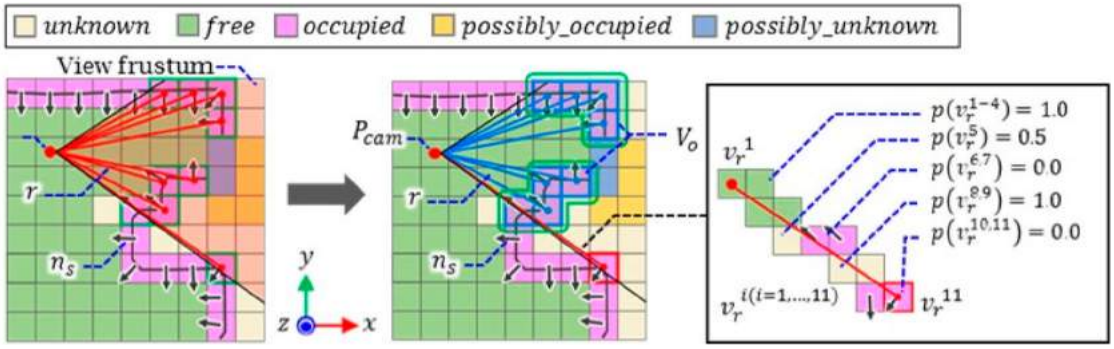

Figure 6. Scan target voxels.

To select the scan target voxel v_{occ}, first, as shown in Fig. 6, a view frustum is generated at each camera position P_{cam} provided by A1. Next, ray casting is performed between every *occupied* voxel v_{occ} with *high* or *middle* priority ($a(v_{occ}) = occupied$ and $b(v_{occ}) \in \{high, middle\}$) in the view frustum and P_{cam}. The voxel v_{occ} on the ray satisfying the following two conditions is finally adopted as the scan target voxel $v_b \in V_o$.

The first is that v_{occ} can be observed from P_{cam}, as expressed by the following equation:

$$\prod_{v_r \in V_r} p(v_r) > 0 \tag{3.1}$$

where $p(v_r)$ is the penetration probability of the extent to which a ray from the camera can penetrate a voxel v_r in the set of voxels V_r that are intersected by the ray r between P_{cam} and v_{occ}.

The penetration probability $p(v_r)$ is set to 1.0 for $a(v_r) = free$, 0.0 for $a(v_r) = occupied$, and 0.5 for $a(v_r) = unknown$. Moreover, based on the setting of spatial occupancy attributes described in Section 3.3, we assign an average probability of 0.5, which lies between the probabilities of *occupied* (0.0) and *free* (1.0) voxel, to voxels with $a(v_r) = possibly\_occupied$, and assign an average probability of 0.75, which lies between the probabilities of *unknown* (0.5) and *free*(1.0), to voxels with $a(v_r) = possibly\_unknown$.

The second is that the incident angle of r, which equals the angle between r and $\boldsymbol{n_s}$, must be less than 90°, where $\boldsymbol{n_s}$ denotes the average normal of the faces in a voxel. This condition shows that the surface area of the SfM model included in the voxel is oriented toward the camera position.

3.7. Estimation of near-optimal scanner placement (A6)

Ideally, the optimal scanner placement in our problem setting is an ordered sequence of scanner setup positions S_{seq} that maximizes the number of measurable voxels in a set of scan target voxels V_o and minimizes the number of scans. The setup position is selected from the candidate scanner position voxels V_c. Every setup position must satisfy the constraints on factors influencing scan quality, namely, incident angle, scan range, and scan overlap, as well as the visibility condition.

Thus, the ideal optimal scanner placement can be formulated as a combinatorial optimization problem with the following constraint conditions (Eqn. (3.2)):

$$\begin{aligned} & \underset{S_{seq} \subset V_c}{maximize} \left| \bigcup_{s_j \in S_{seq}} V_o'(s_j) \right| \\ & \underset{S_{seq} \subset V_c}{minimize} |S_{seq}| \\ subject\ to \quad & C_{ang}(s_j, v_b) \wedge C_{range}(s_j, v_b) \\ \forall v_b \in V_o'(s_j) \subset V_o, \quad & \wedge C_{ovlp}(s_j) \wedge C_{vis}(s_j, v_b) \end{aligned} \tag{3.2}$$

where $S_{seq} = \{s_1, s_2, \ldots, s_M\}$ is an ordered set (sequence) of M scanner setup positions and $s_j \in S_{seq}$ denotes the jth scanner position, which takes one of the centers of the candidate scanner position voxels V_c.

$V'_o(s_j)$ is a subset of the scan target voxels V_o consisting only of the voxels that satisfy the constraints. $C_{ang}(s_j, v_b)$, $C_{range}(s_j, v_b)$, $C_{ovlp}(s_j)$, and $C_{vis}(s_j, v_b)$ are Boolean functions expressing whether the constraints on incident angle, scan range, and scan overlap, as well as the visibility condition, hold when the laser beam enters from a scanner position s_j into a target voxel v_b. Each of the Boolean functions is defined as follows:

1) The incident angle condition $C_{ang}(s_j, v_b)$ is *true* if the constraint given by Eqn. (3.3) is satisfied:

$$\text{ang}\{r(s_j, v_b), \boldsymbol{n_s}(v_b)\} \leq \theta_\alpha \tag{3.3}$$

where $r(s_j, v_b)$ denotes a line connecting s_j and v_q and θ_α is the maximum allowable incident angle.

2) The scan range condition $C_{range}(s_j, v_b)$ is *true* if the constraint given by Eqn. (3.4) is satisfied:

$$d_{min} < \text{dist}(s_j, v_b) \leq d_{max} \tag{3.4}$$

where $\text{dist}(s_j, v_b)$ denotes the distance between s_j and v_b and d_{min} and d_{max} represent the minimum and the maximum allowable scan range distances, respectively.

3) The scan overlap condition $C_{ovlp}(s_j)$ is *true* if the constraint given by Eqn. (3.5) is satisfied:

$$\frac{|V_{occ}(s_{j-1}) \cap V_m(s_j)|}{|V_m(s_j)|} \geq \tau_o \tag{3.5}$$

where $V_{occ}(s_{j-1})$ denotes the union of the occupied voxels captured until the $(j-1)$th scan, $V_m(s_j)$ is the subset of occupied voxels captured in the jth scan, and τ_o is the minimum allowable scan overlap ratio.

4) The visibility condition $C_{vis}(s_j, v_b)$ is *true* if the constraint given by Eqn. (3.6) is satisfied:

$$\prod_{v_l \in V_l} p(v_l) > 0 \tag{3.6}$$

where $p(v_l)$ is the probability of the extent to which a laser beam l from the scanner can penetrate voxel v_l in the set of voxels V_l that are intersected by the laser beam l between s_j and v_b. The probability value $p(v_l)$ is assigned in the same way as that described in Section 3.6.

The voxels v_b that are assigned high priority need to be measured with high accuracy, and the objects assigned *middle* priority need to be measured with an accuracy lower than that corresponding to *high* priority. Therefore, as indicated in Table 2, we assigned upper and lower bound values to the above constraints depending on the scanning priority levels assigned to each voxel.

Unfortunately, the ideal optimization problem given by Eqn. (3.2) has two contradictory objective functions, and it is difficult to solve in a practical setting owing to combinatorial explosion. Therefore, in this study, we only respect the first objective function and reformulate the problem as follows (Eqn. (3.7)):

$$\begin{aligned} & \underset{S_{seq} \subset V_c}{maximize} \left| \bigcup_{s_j \in S_{seq}} V'_o(s_j) \right| \\ \textit{subject to} \quad & C_{ang}(s_j, v_b) \wedge C_{range}(s_j, v_b) \\ \forall v_b \in V'_o(s_j) \subset V_o, \quad & \wedge C_{ovlp}(s_j) \wedge C_{vis}(s_j, v_b) \end{aligned} \tag{3.7}$$

This maximization problem given by Eqn. (3.7) cannot be reduced to the optimization problem of well-known classes, and there is no elaborate algorithm to search for a global optimum solution. Therefore, in this study, we have adopted the following greedy algorithm with a stopping condition on coverage to obtain a near-optimal solution:

(1) Initialize the order index $j \leftarrow 1$ and an ordered set $S_{seq} \leftarrow \{\ \}$.

(2) Find the jth near-optimal scanner position $\widetilde{s_j}$ among V_c which maximizes the number of voxels included in $V'_o(s_j)$ as Eqn. (3.8).

$$\widetilde{s_j} = \arg \left\{ \underset{s_j \in V_c}{maximize} \, |V'_o(s_j)| \right\} \tag{3.8}$$

(3) Insert $\widetilde{s_j}$ into the jth element in the ordered setS_{seq}, and update V_c as $V_c \leftarrow V_c - \{\widetilde{s_j}\}$

(4) If the total number of actually measured scan target voxels $|V_m(s_j)|$ meets the criterion $|V_m(s_j)|/|V_o| \leq \tau_c$, stop the algorithm and output S_{seq} as a near-optimal ordered sequence of scanner setup positions, where τ_c is a prespecified threshold of the climb rate. Otherwise, $j \leftarrow j+1$, and repeat (1) ~ (3)

The stopping condition in this algorithm aims to obtain an efficient sequence with fewer setup positions and prevents the total number of scans from increasing unnecessarily.

4. Results

4.1. Optimal scanner placement for small-scale boiler room

4.1.1. Object to be scanned, condition setting, and optimal scanner placement

In the first experiment, HVAC equipment, ducts, and piping objects in a boiler room ($6.3 \times 6.8 \times 4.6$ m^3) were selected as the target objects to be scanned and modeled. First, as shown in Fig. 7(a), an SfM model of the space

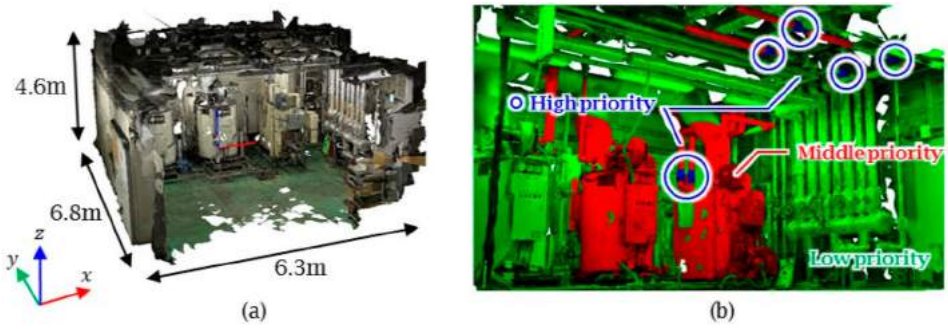

Figure 7. SfM model of boiler room: (a) overview of SfM model and (b) assignment of each scanning priority level.

Table 1. Scanning condition used.

Scanning condition	Value
Scanner height (h_{scan})	1.4 [m]
Scanner base radius (r_{scan})	0.3 [m]
Vertical field of view	320 [deg]
Horizontal field of view	360 [deg]
Vertical scan pitch	0.072 [deg]
Horizontal scan pitch	0.072 [deg]

to be scanned was constructed from 153 pictures taken during a preliminary survey by using commercial SfM software [7]. There are three boilers in this room, and pipes and other facilities are arranged on the top and the side of the room, respectively.

Next, as shown in Fig. 7(b), scanning priority levels are assigned to a few regions on the SfM model. Several flanges connecting the equipment and pipes are assigned *high* priority, regions around the boilers are assigned *middle* priority, and the other regions are assigned *low* priority. The scanning condition of the commercial TLS [9] given in Tab. 1 was used in the proposed NBV method. Different scanners can be simulated by changing these settings. The voxel resolution l_v was set to 0.05 m.

To verify the effectiveness of the proposed method, optimal scanner placements were obtained using the proposed NBV method (Case 1), using an unconstrained NBV method (Case 2), and by an experienced operator (Case 3). The differences in constraint settings in terms of the incident angle, scan range, and scan overlap ratio are summarized in Tab. 2. The proposed NBV method (Case 1) yielded near-optimum scanner placement that completely complied with the constraint settings according to different scanning priority levels (*high* and *middle*). By contrast, the unconstrained NBV method (Case 2) yielded a scanner placement that only complied with the visibility constraint given by Eqn. (3.5) and loose constraint settings, which ignore the scanning priority level. The threshold of climb rate τ_c was set to 0.01.

In Case 3, an experienced operator was asked to place the scanner so that the regions of *high* and *middle* priority specified in Case 1 could be measured, and the regions of *high* priority level could be measured with high accuracy. Namely, the operator (Case 3) determined the scanner setup positions by using the same policy as in Case1. Then, his actual scanner setup positions were captured using a Total Station, imported into our developed NBV software, and a scan simulation was executed from these positions.

Fig. 8 shows a comparison of the scanner placements obtained in Cases 1, 2, and 3. The numbers of scanner setup positions were nine, five, and six, respectively. The time taken by the proposed method to compute the near-optimal scanner placement (Case 1) was 3.5 min when using a standard PC (CPU: Core i7 2.8 GHz, RAM: 32 GB), except for the manual processes of A1 and A3, and that taken by the unconstrained NBV method (Case 2) was 4.1 min.

4.1.2. Effects of constraints according to scanning priority levels

To verify how the proposed scanning-priority-level-based constraints on the incident angle, scan range, and scan overlap ratio affect the final scanner placement, the results obtained using the proposed NBV method

Table 2. Constraint setting.

	Proposed NBV method (Case 1) Scanning priority level		Unconstrained NBV method (Case 2) Scanning priority level
Constraints	High	Middle	Loose
Max. incident angle (θ_α)	45 [deg]	90 [deg]	90 [deg]
Min. scan range (d_{min})	0.3 [m]	0.3 [m]	0.3 [m]
Max. scan range (d_{max})	5.0 [m]	8.0 [m]	20.0 [m]
Min. scan overlap (τ_o)	20.0 [%]	20.0 [%]	0.0 [%]

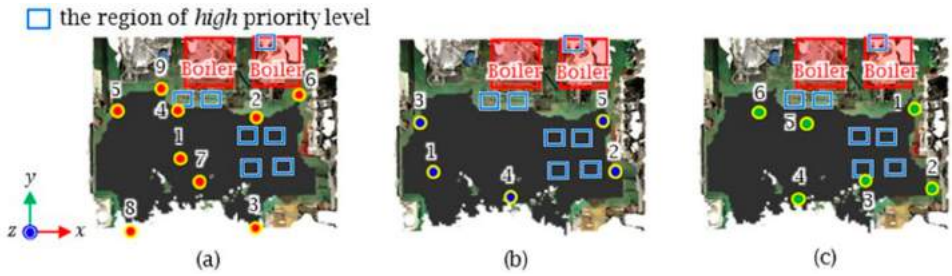

Figure 8. Scanner placement in boiler room obtained by (a) the proposed NBV method (Case 1), (b) unconstrained NBV method (Case 2), and (c) experienced operator (Case 3).

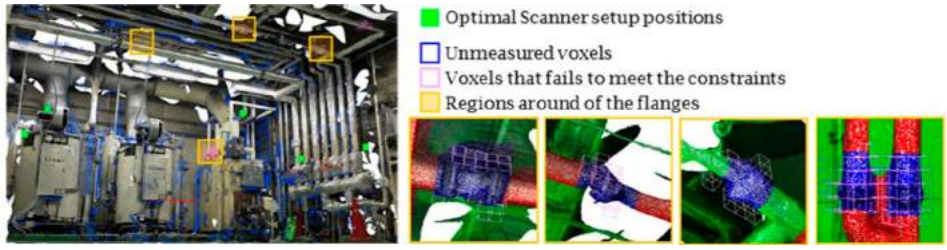

Figure 9. Distribution of voxels not meeting constraints in Case 2 in boiler room.

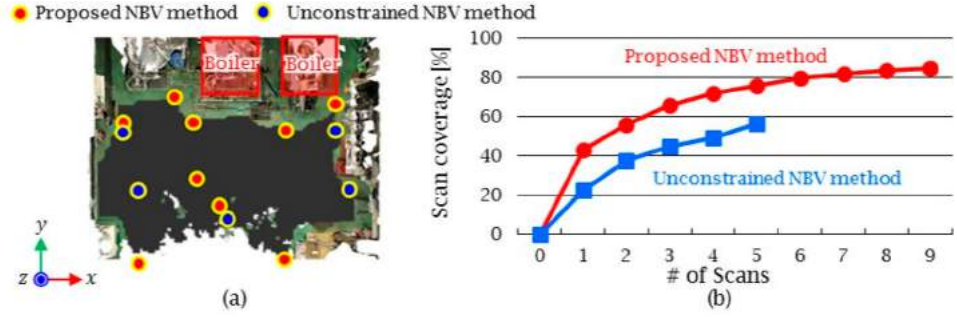

Figure 10. Comparison of the proposed NBV method (Case 1) and unconstrained NBV method (Case 2) in boiler room: (a) Scanner placement and (b) change in scan coverage of voxels meeting the constraints for each scan.

(Case 1) were compared with those obtained using the unconstrained NBV method (Case 2).

As shown in Fig. 8(a) and (b) or in Fig. 10(a), in the proposed NBV method, the scanner is placed closer to the center of the room and closer to the region of *high* priority than in the unconstrained NBV method, and there are four more scanner setup positions than in the unconstrained NBV method. The coverage of *high* priority voxels reached 85.0% in the 9th scan in Case 1 and 97.0% in the fifth scan in Case 2. From the comparison, Case 2 appears to be superior to Case 1 in terms of voxel coverage.

However, as shown in Fig. 9, many voxels fail to meet the constraints when using the scanner placement obtained using the unconstrained NBV method (Case 2). The ratio of failed voxels to wholly measured voxels reached 41.6%, and particularly, the failed voxels are distributed widely on the flanges. Fig. 10(b) shows the coverage of voxels that meet the constraints of Cases 1 and 2 only. The voxel coverage in Case 2 decreased to 56.7% even after the fifth scan, while that obtained by the proposed NBV method (Case 1) remained at 85.0%. Moreover, in every scan, the coverage of Case 1 was superior to that of Case 2. Consequently, by applying the constraints, we could determine effective scanner placement for precise scanning that satisfied the scan quality requirements. The scanning-priority-level-based constraints on the incident angle, scan range, and scan overlap ratio introduced in the proposed NBV method are indispensable for obtaining scanner placement that guarantees *high* scan quality.

4.1.3. Comparison with scanner placement by an experienced operator

The scanner placement obtained using the proposed NBV method (Case 1) was compared with that made by an experienced scanner operator (Case 3). The operator is a professional who has executed more than 100

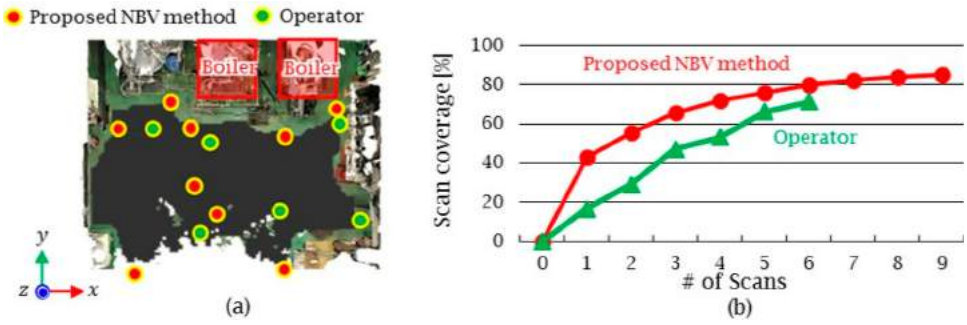

Figure 11. Comparison of the proposed NBV method (Case 1) and experienced operator (Case 3) in boiler room: (a) scanner placement and (b) change in scan coverage of voxels meeting constraints for each scan.

scanning projects over four years and has experience in managing the construction of HVAC facilities.

At the start of the experiment, the operator was asked to scan as many surfaces on the objects in the environment as possible and asked to adhere to the scan quality requirements (constraints on distance, incident angle, and overlap) at the same time. In addition, we confirmed that the operator adhered to the constraints during the scan and that the scanning operation was not very different from a typical scanning operation.

As shown in Fig. 11(a), the operator obtained four fewer scanner setup positions than those obtained using the proposed NBV method. The coverage of *high* priority voxels was 93.6% in Case 3, which appears to be superior to that in Case 1.

However, as in Section 4.1.2, in Case 3, 23.9% of the voxels failed to meet the constraints. As shown in Fig. 11(b), voxel coverage satisfying the constraints decreased to 71.2% when the scanner was placed by the operator (Case 3). The coverage obtained using the proposed NBV method (Case 1) was superior to that obtained by the experienced operator (Case 3) in every scan. As a result, the proposed NBV method can yield better scanner placement than that obtained by the experienced operator, thus guaranteeing higher scan quality.

4.2. Optimal scanner placement for middle-scale heat source machine room

4.2.1. Object to be scanned, condition setting, and optimal scanner placement

In the second experiment, to verify that the proposed method functions correctly in larger and more complex environments, HVAC equipment, ducts, and piping objects in a heat source machine room (12.1 × 14.1 × 4.6 m^3) were selected as the target objects to be scanned and modeled. First, as shown in Fig. 12(a), an SfM model of the space to be scanned was constructed from 486 pictures. As shown in Fig. 12(b), there is an absorption chiller in the center of this room, and pipes and other facilities are arranged densely on the top and the side of the room, respectively.

Next, as shown in Fig. 12(b), scanning priority levels are assigned to a few regions on the SfM model. Several flanges connecting the equipment and pipes are assigned *high* priority, regions around the chiller are assigned *middle* priority, and the other regions are assigned *low* priority. The scanning condition was set to be the same as that in the first experiment, as summarized in Tab. 1. The voxel resolution l_v was set to 0.05 m.

As in Section 4.1, to verify the effectiveness of the proposed method, optimal scanner placements were

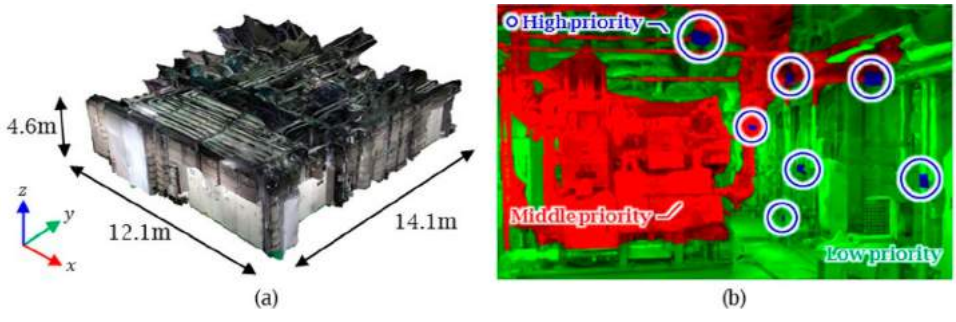

Figure 12. SfM model of heat source machine room: (a) overview of SfM model and (b) assignment of each scanning priority level.

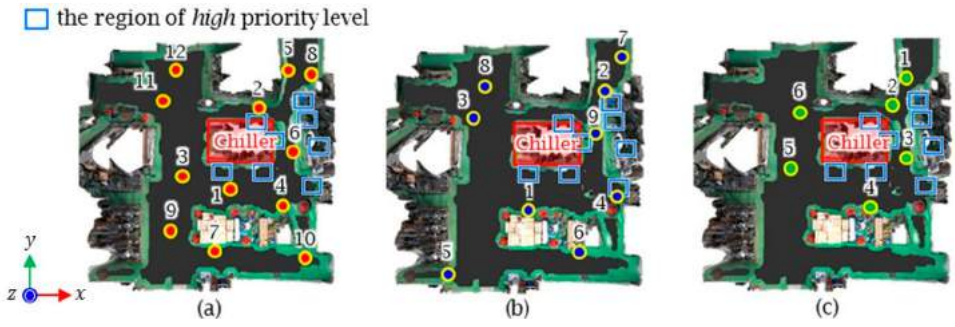

Figure 13. Scanner placement in heat source machine room obtained by (a) the proposed NBV method (Case 1), (b) unconstrained NBV method (Case 2), and (c) experienced operator (Case 3).

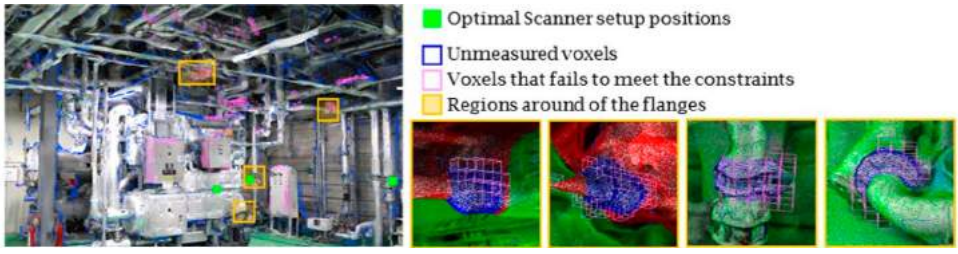

Figure 14. Distribution of voxels not meeting constraints in Case 2 in heat source machine room.

obtained using the proposed NBV method (Case 1), using the unconstrained NBV method (Case 2), and by an experienced operator (Case 3). The policy for determining the scanner placement in each case is the same as that described in Section 4.1.1, and the constraint settings are the same as those summarized in Tab. 2. The threshold of the climb rate τ_c was set to 0.01.

Fig. 13 shows a comparison of the scanner placements obtained in Cases 1, 2, and 3. The numbers of scanner setup positions were twelve, nine, and six, respectively. The time taken by the proposed method to compute the near-optimal scanner placement (Case 1) was 50.9 min when using the same PC, except for the manual processes of A1 and A3, and that taken by the unconstrained NBV method (Case 2) was 49.8 min. Therefore, we confirmed that the proposed method functions correctly in larger and more complex environments.

4.2.2. Effects of constraints according to scanning priority levels

As in Section 4.1.2, to verify how the proposed scanning-priority-level-based constraints on the incident angle, scan range, and scan overlap ratio affect the final scanner placement, the results obtained using the proposed NBV method (Case 1) were compared with those obtained using the unconstrained NBV method (Case 2).

As shown in Fig. 13(a) and 13(b) or in Fig. 15(a), in the proposed NBV method, the scanner is placed closer to the region of *high* priority than in the unconstrained NBV method, and there are three more scanner setup positions than in the unconstrained NBV method. The coverage of *high* priority voxels was 88.0% in the 12th scan in Case 1 and 95.3% in the 9th scan in Case 2.

However, as shown in Fig. 14, many voxels fail to meet the constraints when using the scanner placement obtained with the unconstrained NBV method (Case 2). The ratio of failed voxels to wholly measured voxels was 27.0%. Fig. 15(b) shows the coverage of voxels that meet the constraints of Cases 1 and 2 only. The voxel coverage in Case 2 decreased to 69.6% even after the 9th scan, while that obtained using the proposed NBV method (Case 1) remained at 88.0%. Moreover, in every scan, the coverage of Case 1 was superior to that of Case 2. Therefore, even in larger and more complex environments, by applying the constraints, we could determine effective scanner placement to achieve precise scanning that satisfies the scan quality requirements.

4.2.3. Comparison with scanner placement by an experienced operator

As in Section 4.1.3, the scanner placement obtained using the proposed NBV method (Case 1) was compared with the scanner placement by an experienced scanner operator (Case 3). As shown in Fig. 16(a), the operator obtained half the number of scanner setup positions as those obtained by using the proposed NBV method. A few setup positions in Cases 1 and 3 were located close to each other. The coverage of *high* priority voxels was 88.9% in Case 3, which appears to be superior to that in Case 1.

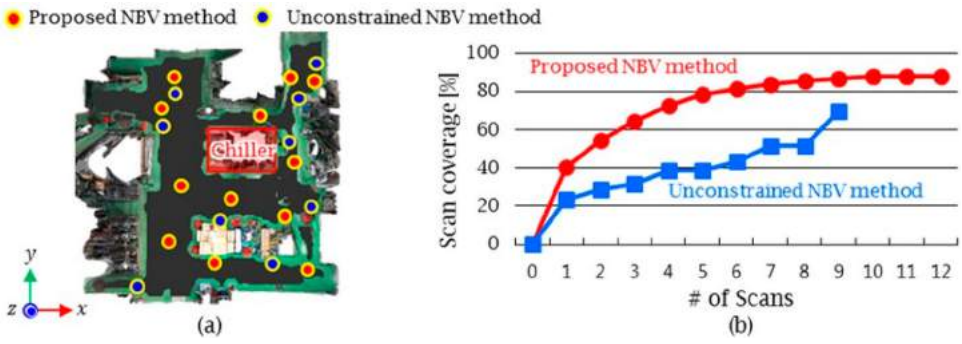

Figure 15. Comparison of the proposed NBV method (Case 1) and unconstrained NBV method (Case 2) in heat source machine room: (a) scanner placement and (b) change in scan coverage of voxels meeting the constraints for each scan.

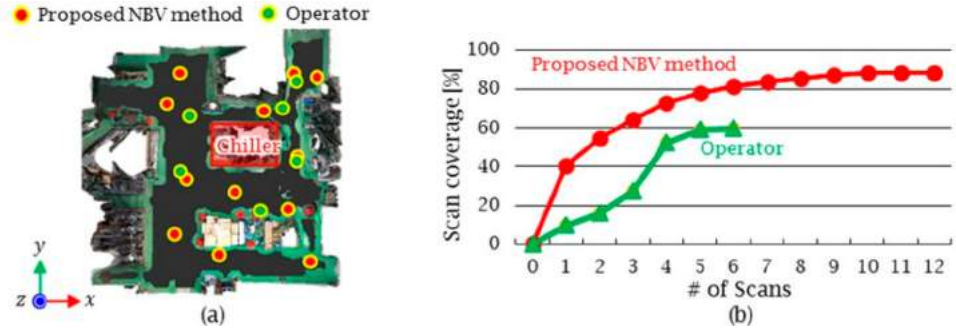

Figure 16. Comparison of the proposed NBV method (Case 1) and experienced operator (Case 3) in heat source machine room: (a) scanner placement and (b) change in scan coverage of voxels meeting the constraints for each scan.

However, as in Section 4.2.2, in Case 3, 33.0% of the voxels failed to meet the constraints. As shown in Fig. 16(b), voxel coverage satisfying the constraints decreased to 59.6% when the scanner was placed by the operator (Case 3). The coverage obtained using the proposed NBV method (Case 1) was superior to that obtained by the experienced operator (Case 3) in every scan. As a result, even in larger and more complex environments, the proposed NBV method can yield better scanner placement, which guarantees higher scan quality than that obtained by the experienced operator.

4.2.4. Quantitative evaluation of scanning accuracy

Finally, we evaluated the effectiveness of the optimal scanner placement obtained using the proposed NBV method in terms of increasing the accuracy of as-built 3D modeling. The dimensional and positional accuracies of several flange models generated from the scanned points captured using the proposed NBV method (Case 1) were compared with those of the models generated using the other two approaches (Cases 2 and 3).

First, the optimum scanner setup positions estimated using the NBV methods (Cases 1 and 2) were converted to real-space coordinates. Then, these setup positions were pointed on the floor by a laser beam irradiated from a Total Station, and the TLS was placed at those positions. Multiple scan data were registered using commercial point-cloud-processing software [9]. The diameters and positions of several flanges to which *high* priority level was assigned were evaluated. Fig. 17 shows the positions of these flanges in the SfM model. The diameters of the flanges and the center positions of their end faces were evaluated. From the registered point clouds, only the point clouds placed on the cylindrical surfaces and their end faces were segmented manually. Cylinders with end faces were finely fit to the segmented point clouds by using the Levenberg–Marquardt method [18] and the least-squares method to estimate the diameters and the center positions of the end faces. The diameters and positions measured using the Total Station were taken as reference values. Three points on the circumference of each flange were measured using a specialized jig with a prism for flange measurement, and the real diameters and positions were calculated.

Fig. 18(a) and 18(b) show comparisons of the errors in the diameters and center positions, respectively, of the end faces of the as-built flange models. These models were generated using the point clouds obtained from the scanner positions determined using the three methods (Cases 1, 2, and 3). As shown in Fig. 18(a), the mean errors in the diameters calculated using each of the methods are 1.32 mm (Case 1), 6.39 mm (Case 2),

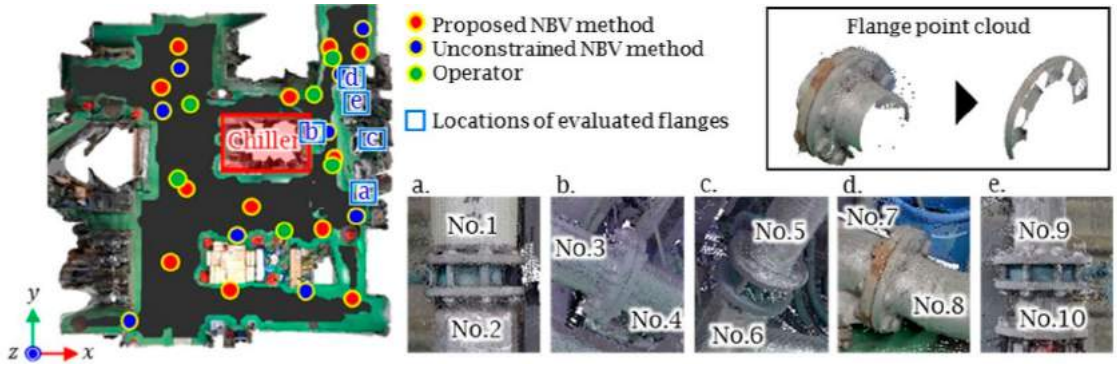

Figure 17. Distribution of voxels not meeting constraints in Case 2 in heat source machine room.

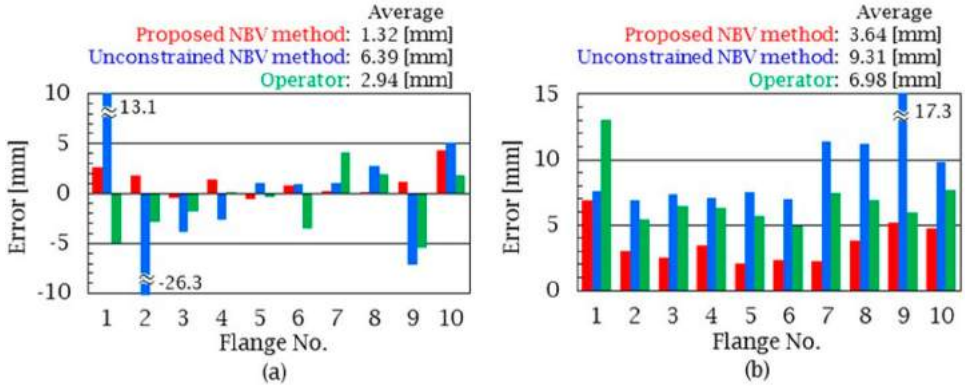

Figure 18. Measurement error in case of flanges in heat source machine room: (a) diameter and (b) center position of end face.

and 2.94 mm (Case 3), respectively. Since the diameters of off-the-shelf flanges are provided in intervals of 5 to 15 mm in the JISB2220 [11], the diameter error must be 5 mm or lower. As shown in Fig. 18 (a), all the diameter errors in Case 1 fall within this allowance (5 mm). So, we can identify correctly the standard diameters of existing flanges using the point clouds in Case 1. Moreover, when replacing an existing pipe with a new one by using the prefabrication method, the position error must be 5 mm or lower. As shown in Fig. 18(b), the mean errors in the center position of the end face are 3.64 mm (Case 1), 9.31 mm (Case 2), and 6.98 mm (Case 3), respectively. Moreover, most of the positional errors in Case 1 fall within this practical allowance (5 mm). Thus, we can confirm that the proposed NBV method is effective for achieving the required scan quality and increasing the accuracy of as-built 3D modeling.

5. Conclusions

In this paper, we proposed a new model-based NBV planning method for TLSs by using a coarse 3D model constructed from SfM as *a priori* knowledge. The method can estimate near-optimum scanner placement that maximizes scan coverage while satisfying the constraints on the factors influencing scan quality, such as beam incident angle, scan range, and scan overlap, based on voxelization of the space to be scanned and ray casting inside voxels. The constraints could be controlled based on user-specified scanning priority levels that reflect the differences in the degree of scan quality according to the construction type. Near-optimum scanner placement was determined within a reasonable processing time by using a greedy method. The estimation results show that the proposed NBV method can output a scanner placement with better scan coverage than that achieved by the unconstrained NBV method and an experienced operator, while strictly satisfying the scan-quality-related constraints. Moreover, we confirmed that the proposed NBV method is effective for achieving better scan quality, which improves the accuracy of as-built 3D modeling, compared to that achieved by the unconstrained NBV method and an experienced operator. The results suggest that the proposed method enables inexperienced operators to easily capture laser-scanned points with the required scan quality for construction.

In the future, we will explore more efficient and optimal scanner placement by using a global optimization method and improve the method of constructing a coarse model by using capturing technologies other than SfM.

ORCID

Eisuke Wakisaka http://orcid.org/0000-0002-2881-8010
Satoshi Kanai http://orcid.org/0000-0003-3570-1782
Hiroaki Date http://orcid.org/0000-0002-6189-2044

References

[1] Ahmed, M. F.; Haas, C. T.; Haas, R.: Automatic detection of cylindrical objects in built facilities, Journal of Computing in Civil Engineering, 28(3), 2014, 04014009. https://doi.org/10.1061/(asce)cp.1943-5487.0000329
[2] Ahn, J.; Wohn, K.: Interactive scan planning for heritage recording, Multimedia Tools and Applications, 2016, 1–21. http://doi.org/10.1007/s11042-015-2473-0
[3] Bapat, A.; Ravi, A.; Raman, S.: An iterative, non-local approach for restoring depth maps in RGB-D images, Communications (NCC), 2015 Twenty First National Conference on. IEEE, 2015, 1–6. http://doi.org/10.1109/NCC.2015.7084819
[4] Blaer, P. S.; Allen, P. K.: View planning and automated data acquisition for three-dimensional modeling of complex sites, Journal of Field Robotics, 26(11-12), 2009, 865–891. https://doi.org/10.1002/rob.20318
[5] Boehler, W.; Vicent, M. B.; Marbs, A.: Investigating laser scanner accuracy, The International Archives of Photogrammetry, Remote Sensing and Spatial Information Sciences, 34(Part 5), 2003, 696–701.
[6] Chen, M.; Soibelman. L.; Becerik, G. B.: A proactive Scan Planning Framework for Courtyard-Centric Buildings, Proceedings of the 16th International Conference on Civil and Building Engineering Informatics, 2016, 1444–1451.
[7] ContextCapture, https://www.bentley.com/en/products/brands/contextcapture, Bentley.
[8] Heidari, M. M.; Varshosaz, M.: Optimal placement of a terrestrial laser scanner with an emphasis on reducing occlusions, The Photogrammetric Record, 31(156), 2016, 374–393, http://dx.doi.org/10.1111/phor.12162
[9] Imager5010C, http://zf-laser.com/Z-F-IMAGER-R-5010C.3d_laserscanner.0.html?&L-1, Zoller + Fröhlich.
[10] InfiPoints, http://elysium-global.com/productinfo/infipoints/, Elysium.
[11] JISB2220, Steel pipe flanges, Japanese Standards Association, 2004.
[12] Kitada, Y.; Dan, H.; Yasumuro, Y.: Optimization scenario for 3D-scanning plans of outdoor constructions based on SFM, Proceedings of the 15th International Conference on Construction Applications of Virtual Reality, 2015, 65–68.
[13] Kawashima, K.; Yamanishi, S.; Kanai, S.; Date, H.: Finding the next-best scanner position for as-built modeling of piping systems, The International Archives of the Photogrammetry Remote Sensing and Spatial Information Sciences, KL-5, 2014, 313–320. https://doi.org/10.5194/isprsarchives-xl-5313-2014
[14] Kersten, T.; Mechelke, K.; Lindstaedt, M.; Sternberg, H.: Geometric accuracy investigations of the latest terrestrial laser scanning systems, Integrating Generations, FIG Working Week 2008, 2008.
[15] Narumi, M.; Kanai, S.; Date, H.; Wakisaka, E.; Sakamoto, S.: Laser-scanned as-built 3D modeling of air-conditioning ducts based on Manhattan world assumption, 15th International Conference on Computing in Civil and Building Engineering, 2016, Paper ID:287.
[16] Pito, R.: A solution to the next best view problem for automated surface acquisition, IEEE Transactions on Pattern Analysis and Machine Intelligence, 21(10), 1999, 1016–1030. https://doi.org/10.1109/34.799908
[17] Scott, W. R.; Roth, G.; Rivest, J. F.: View planning for automated three-dimensional object reconstruction and inspection, ACM Computing Surveys (CSUR), 35(1), 2003, 64–96. https://doi.org/10.1145/641865.641868
[18] Shakarji, C. M.: east-squares fitting algorithms of the NIST algorithm testing system, Journal of research of the National Institute of Standards and Technology, 103(6), 1998, 633–641. https://doi.org/10.6028/jres.103.043
[19] Soudarissanane, S.; Lindenbergh, R.; Menenti, M.; Teunissen, P.: Incidence angle influence on the quality of terrestrial laser scanning points, International Society for Photogrammetry and Remote Sensing, 2009, 183–188.
[20] Soudarissanane, S.; Lindenbergh, R.: Optimizing terrestrial laser scanning measurement set-up, International Archives of the Photogrammetry, Remote Sensing and Spatial Information Sciences, Volume XXXVIII-5/W12, 2011, 127–132. https://doi.org/10.5194/isprsarchives-xxxviii-5-w12-127-2011
[21] Svensson, M.: Accelerated Volumetric Next-Best-View Planning in 3D Mapping, Ph.D. Thesis, Linköping University, 2014.
[22] Wujanz, D.; Holst, C.; Neitzel, F.; Kuhlmann, H.; Niemeier, W.; Schwieger, V.: Survey configuration for terrestrial laser scanning, Allgemeine Vermessungsnachrichten (AVN), 6(2016), 2016, 158–169.